NANO LETTERS

2008
Vol. 8, No. 7
2063-2069

Induction of Cell Polarization and Migration by a Gradient of Nanoscale Variations in Adhesive Ligand Spacing

Marco Arnold,[†,‡] Vera C. Hirschfeld-Warneken,[†,‡] Theobald Lohmüller,[‡] Patrick Heil,[‡] Jacques Blümmel,[‡] Elisabetta A. Cavalcanti-Adam,[‡] Mónica López-García,[§] Paul Walther,[||] Horst Kessler,[§] Benjamin Geiger,[⊥] and Joachim P. Spatz*[,‡]

Department of New Materials and Biosystems, Max Planck Institute for Metals Research, and Department of Biophysical Chemistry, University of Heidelberg, Heisenbergstr. 3, D-70569 Stuttgart, Germany, Center of Integrated Protein Science Munich at the Technical University of Munich, Department Chemie, Technical University of Munich, Lichtenbergstrasse 4, D-85747 Garching, Germany, Central Unit for Electron Microscopy, University of Ulm, Albert-Einstein-Allee 11, D-89069 Ulm, Germany, Department of Molecular Cell Biology, Weizmann Institute of Science, Rehovot 76100, Israel

Received May 23, 2008

ABSTRACT

Cell interactions with adhesive surfaces play a vital role in the regulation of cell proliferation, viability, and differentiation, and affect multiple biological processes. Since cell adhesion depends mainly on the nature and density of the adhesive ligand molecules, spatial molecular patterning, which enables the modulation of adhesion receptor clustering, might affect both the structural and the signaling activities of the adhesive interaction. We herein show that cells plated on surfaces that present a molecularly defined spacing gradient of an integrin RGD ligand can sense small but consistent differences in adhesive ligand spacing of about 1 nm across the cell diameter, which is approximately 61 μm when the spacing includes 70 nm. Consequently, these positional cues induce cell polarization and initiate cell migration and signaling. We propose that differential positional clustering of the integrin transmembrane receptors is used by cells for exploring and interpreting their environment, at high spatial sensitivity.

Adhesion of tissue cells to the extracellular matrix depends on the activation of specific transmembrane receptors, for example, integrins, which leads to the assembly of specialized adhesion sites known as focal adhesions (FA).[1] Activation and spatial organization of integrins are mainly controlled by epitopes containing an RGD (R = arginine, G = glycine, D = aspartate) sequence, that is present on a variety of adhesive extracellular matrix (ECM) proteins. Recent studies indicated that, beyond the chemical specificity of the adhesive epitope,[2] many physical features of the adhesive surface, including its geometry,[3] rigidity,[4] and precise epitope spacing,[5] are critical for guiding receptor-mediated adhesion formation and signaling. Specifically, it was demonstrated that cyclic RGDfK[6] peptides linked to nanogold particles which were arranged in pattern on substrates and interspaced by 58 or 73 nm, influence cell adhesion,[5] spreading, focal adhesion assembly, and migration[7,8] in very different ways. In these studies, control experiments demonstrated that only the specific functionalization of nanogold particles with cyclic RGD induced integrin clustering and such focal adhesion formation upon interaction with cells such as 3T3-fibroblasts or -osteoblasts. Nonfunctionalized nanogold particles[5] or nanoparticles that were functionalized with a random sequence of amino acids, that is, arginine, glycine, and glutamic acid (RGE),[9] did not induce adhesion associated cell responses. Even more detailed, blocking of integrin $\alpha v\beta 3$ by antibodies revealed no adhesion response if nanogold particle patterns were functionalized with cyclic RGD.[8]

The number of adhering cells, their morphology, and their alignment are affected by plating the cells on gradients of immobilized fibronectin[10] or RGD peptides.[11] Axon extensions of rat hippocampal neurons[12] and migrating cells[13] tend to preferentially orient toward increasing surface density of

* Corresponding author. E-mail: spatz@mf.mpg.de.
† Both authors contributed equally to this work.
‡ Max Planck Institute for Metals Research and University of Heidelberg.
§ Technical University of Munich.
|| University of Ulm.
⊥ Weizmann Institute of Science.

10.1021/nl801483w CCC: $40.75
Published on Web 06/18/2008

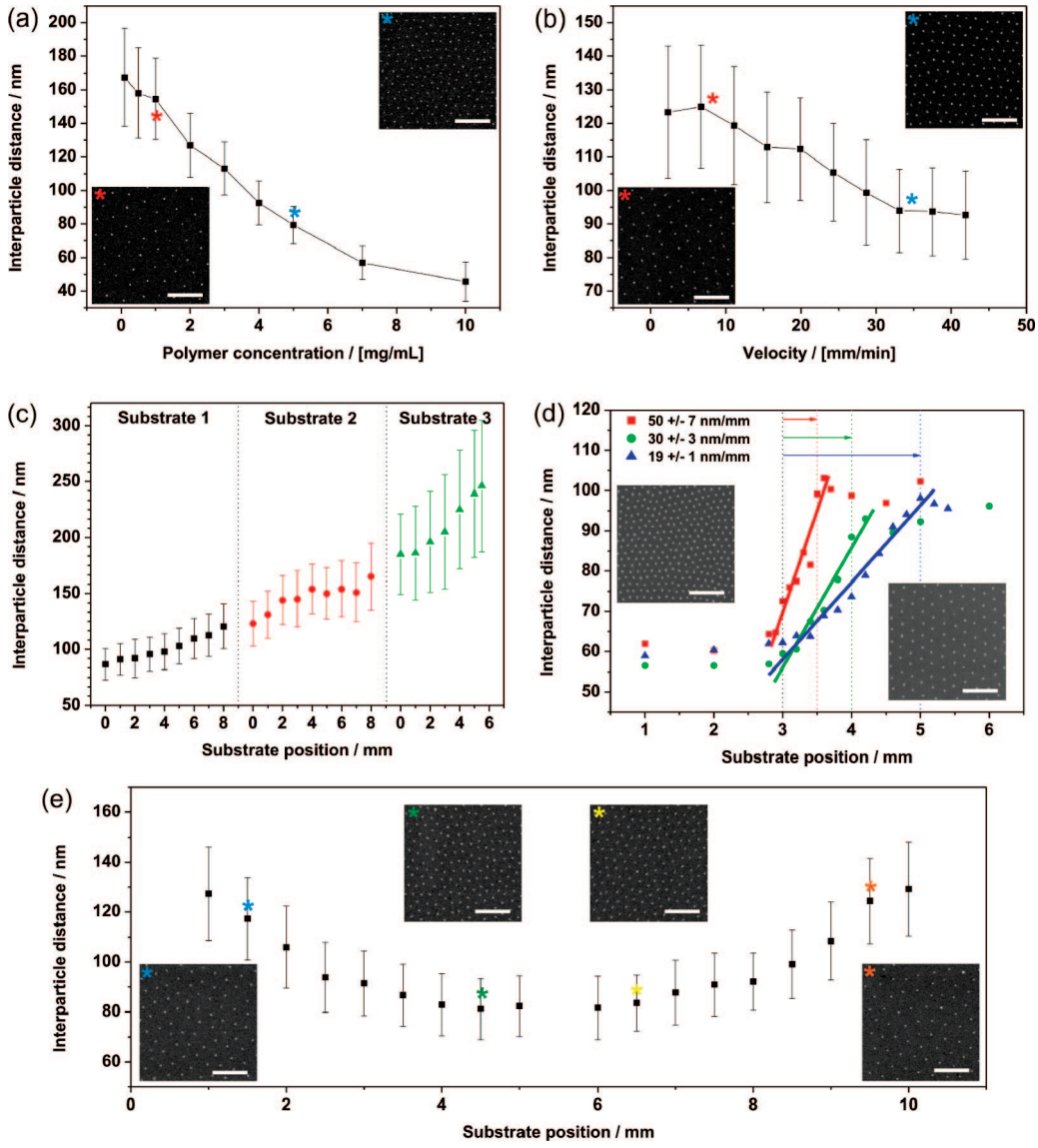

Figure 1. Nanoparticle spacing gradients. Variations in gold nanoparticle spacing along a substrate by using a PS(1780)-*b*-P[2VP($HAuCl_4$)$_{0.2}$](520) diblock copolymer solution as a function of (a) polymer concentration; substrate retraction velocity (v = 12 mm/min) and (b) retraction velocity; polymer solution of 2 mg/mL. (c) Three examples of particle spacing gradients ranging from ~80 to ~250 nm for three different molecular weight diblock copolymers and varying substrate retraction velocities. [Substrate 1: ■ (PS(990)-*b*-P[2VP($HAuCl_4$)$_{0.5}$] (385) (c = 3 mg/mL, v = 40−8 mm/min). Substrate 2: ● PS(1826)-*b*-P[2VP($HAuCl_4$)$_{0.5}$] (523) (c = 2 mg/mL, v = 40−8 mm/min). Substrate 3: ▲ PS(5355)-*b*-P[4VP($HAuCl_4$)$_{0.5}$] (714) (c = 1 mg/mL, v = 30−8 mm/min).] (d) Particle spacing gradients with varying gradient strength of (19 ± 1), (30 ± 3), and (50 ± 7) nm/mm. Gradients were generated from a PS(990)-*b*-P[2VP($HAuCl_4$)$_{0.3}$] (385) diblock copolymer solution of 5 mg/mL. Retraction procedure: (1) 3 mm constant retraction velocity of 40 mm/min; (2) 0.5, 1, or 2 mm gradual deceleration of retraction velocity from 40 to 8 mm/min; (3) constant retraction velocity of 8 mm/min. All scale bars: 300 nm. Error bars = s.d. of measured particle spacing. (e) Particle spacing for two conversely oriented gradients derived from a PS(1780)-*b*-P[2VP($HAuCl_4$)$_{0.2}$] (520) diblock copolymer solution of 2 mg/mL on one substrate plotted against substrate position. The retraction velocity was accelerated from 8 to 40 mm/min for the first gradient (0−5 mm) and decreased from 40 to 8 mm/min for the second gradient (6−10 mm) on a single substrate. The asterisks indicate the insets displaying SEM micrographs of the respective substrate positions. Insets show SEM micrographs of the substrate positions indicated by different asterisks (all scale bars: 300 nm; error bars = standard deviation of measured particle spacing).

the corresponding adhesion molecules. However, despite compelling evidence from local directional cues, generated by variations in density of adhesion molecules, the mechanisms whereby cells sense these variations, as well as specific variations in density, remain unclear.

In recent years, new tools for the generation of surfaces displaying adhesive ligand density gradients have been developed. These techniques include the photoimmobilization of peptides on self-assembled monolayers,[14] microfluidic systems,[15] contact printing,[16] or dip-pen lithography.[17] Gold nanoparticle density gradients may be obtained by assembling the nanoparticles along a concentration gradient of amino groups.[18] More recently, protein-coated gold and silver nanoparticles have been used for the assembly of protein density gradients, by varying the immersion time of the solid support.[19] On the molecular length scale, these methods

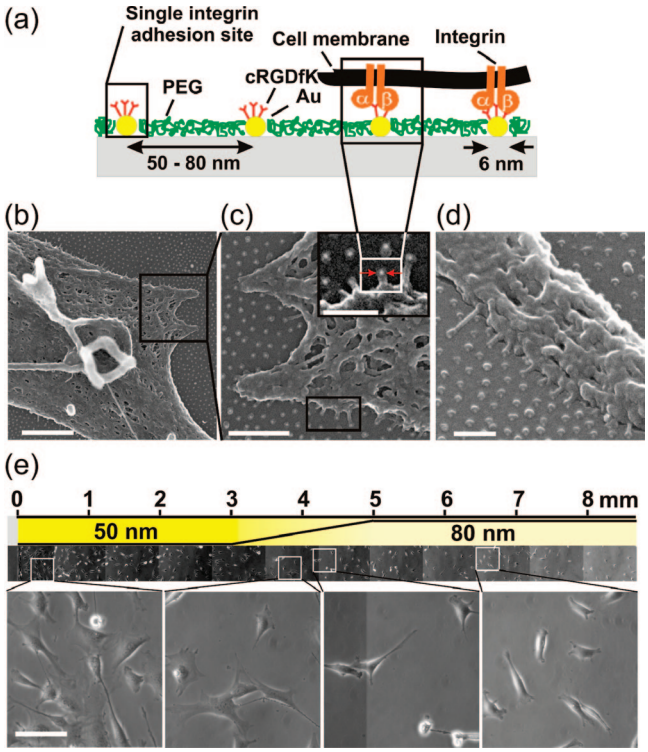

Figure 2. Biofunctionalized particle spacing gradient. (a) Scheme of the biofunctionalized substrate; (b,c) Scanning electron micrographs show parts of critical point-dried MC3T3 osteoblasts plated for 21 h on biofunctionalized nanopatterns of ~60 nm particle separation. The inset in (c) shows a close-up of ultrasmall cellular protrusions with a diameter of ~10 to ~20 nm and a length of ~30 to ~50 nm, interacting selectively with the c(-RGDfK-) functionalized gold nanoparticles which are adhesion patches for single integrin receptors. (d) SE micrograph with a tilt angle of 40° depicts ultrasmall cellular protrusions interacting with integrin adhesion sites. (e) Cells were plated for 21 h on biofunctionalized particle spacing gradient substrates with c(-RGDfK-) patch spacing from 50 to 80 nm, between a 3 and a 5 mm substrate position. Top: Stitched phase-contrast micrograph presenting the adhesion of cells to the different areas of the substrate. Bottom: Close-up of MC3T3 cells on patch spacing, at substrate areas offering ~50, ~60, ~70, and ~80 nm patch spacing. Scale bars: (b) 500 nm, (c) 200 nm (inset: 100 nm), (d) 100 nm, (e) 100 μm.

enable quantification of an average molecular concentration, which gradually varies along the adhesive surface; however, they are too "noisy" to quantify the densities themselves and density variations capable of inducing cell polarization.

We herein demonstrate a novel surface patterning technique for the generation of nanoparticle spacing gradients, which is based on controlled modulation of the self-assembly of diblock copolymer micelles. Because of the self-assembly of macromolecules, large-scale surface areas are easily processed by this technique. After successful biofunctionalization of the nanoparticles with c(-RGDfK-),[5,7,8] each single particle binds up to one integrin.[20] Upon adhesion of cells, the gradual increase in spacing between individual nanoparticles and, thus, local changes in integrin clustering enable the testing of the response sensitivity of cells to the spatial separation of individual adhesion molecules.

Block copolymer micelle nanolithography (BCMN) enables the positioning of 1−15 nm sized gold particles in a quasi-hexagonal pattern, with a tunable particle spacing of 15−250 nm, by dip-coating a substrate, and subsequently subjecting it to a plasma process which removes the entire polymer but, at the same time, deposits gold particles on the substrate in well-defined patterns.[21–24] Varying the molecular weight of diblock copolymers causes variations in lateral spacing between the gold nanoparticles. Here, we demonstrate that the lateral spacing of gold nanoparticles also depends on the concentration of the micellar dip-coating solution and on the substrate retraction velocity, the latter of which enables the formation of well-defined nanoparticle spacing gradients.

Extended and highly regular monomicellar films were prepared by dip-coating Si(100)-wafers or glass coverslips into toluene solutions of polystyrene(x)-*b*-poly(2-vinylpyridine)(y) (PS(x)-*b*-P2VP(y)) diblock copolymers.

Scanning electron microscopy (SEM) was then used to evaluate particle spacing as a function of polymer concentration, revealing a particle spacing for the PS(1780)-*b*-P[2VP($HAuCl_4$)$_{0.2}$](520) diblock copolymer which ranged from ~50 nm for 10 mg/mL to ~170 nm for 0.1 mg/mL, when a substrate was retracted from the solution at a speed of 12 mm/min (Figure 1a). The graph displays a linear decrease in the particle spacing, as the polymer concentration increases from 1 to 5 mg/mL; this decrease saturates toward 50 nm when the polymer concentration reaches 10 mg/mL. The insets in Figure 1a depict two representative SEM micrographs, revealing quasi-hexagonal arrays of gold nanoparticles obtained at polymer concentrations of 1 mg/mL and 5 mg/mL.

The particle spacing was then varied by changing the substrate retraction velocity from 2.3 to 41.9 mm/min, using a 2 mg/mL solution of PS(1780)-*b*-P[2VP($HAuCl_4$)$_{0.2}$](520) diblock copolymer. Increasing the retraction velocity led to a quasi-linear decrease in the particle spacing from approximately 125 to 95 nm (Figure 1b). Notably, a maximal retraction velocity was also observed, above which the particle spacing saturates. This finding is explained by the observation that a faster retraction velocity of the substrate results in a thicker liquid film adsorbed to it, since the liquid has less time to flow back into the solution reservoir. This results in an increased number of deposited micelles per unit area, after evaporation of the solvent. Since a dissolved diblock copolymer micelle consists of a soft shell of polystyrene, micelles adjust to variations in micellar density during solvent evaporation by forming energetically favorable micellar core-to-core spacing, while each core positions the gold for deposition on substrates. Saturation of micellar packing is obtained when the polystyrene shell cannot be condensed any further.

A particle spacing gradient on one substrate was obtained by varying the substrate retraction velocity from the micellar solution. An extended range of particle spacing gradients was obtained by combining the alternation in polymer length with the retraction velocity (Figure 1c). The combination of three different molecular weights of PS-P2VP diblock copolymers with different substrate retraction velocities yielded variations in particle spacing between 80 and 250 nm. In general, a

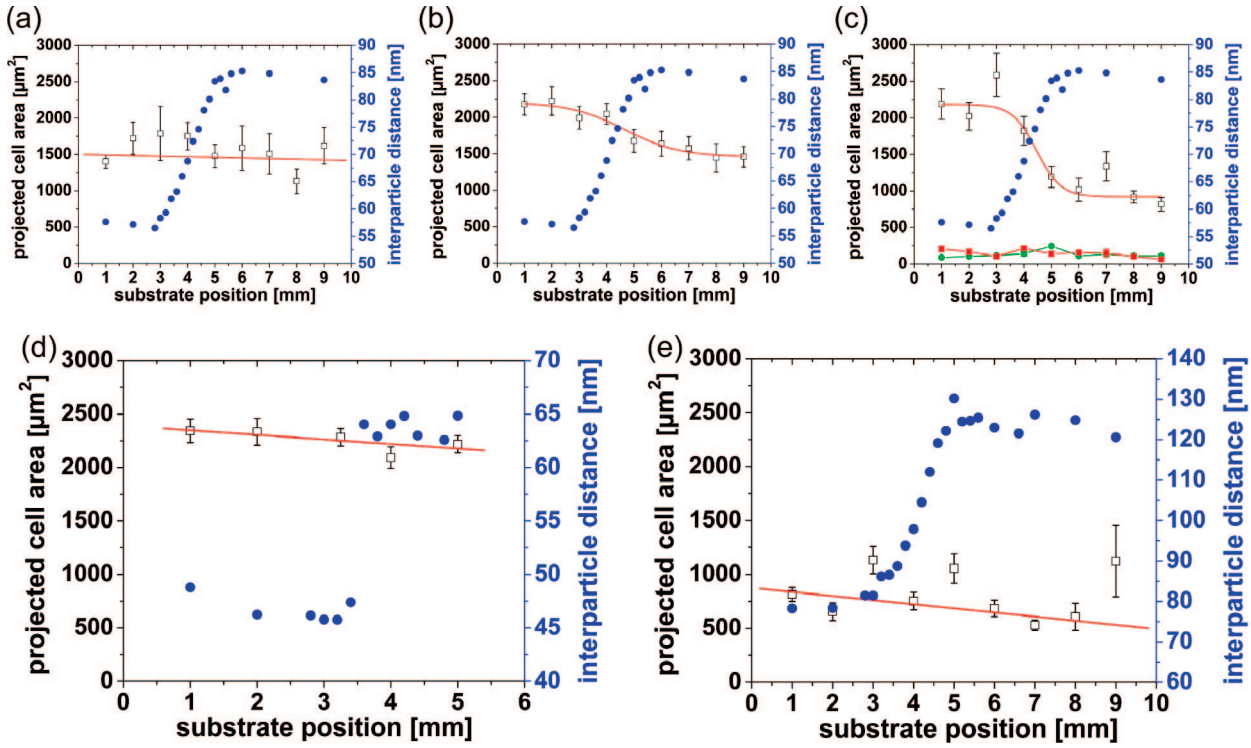

Figure 3. Projected area of cells adhering along gradients covering various ligand patch spacing, strengths, and adhesion times. Ligand patch spacing (●) and projected cell area (□) of cells plated after (a) 2.5 h (248 cells analyzed), (b) 8 h (159 cells analyzed), and (c) 23 h (200 cells analyzed) as a function of substrate position, with a gradient strength of Δ15 nm/mm each. Control experiments with nonfunctionalized nanogold particles (red squares) and particles that were functionalized with RGE-peptides (green circles) proved the specificity of cell responses due to c(-RGDfK-) functionalization. Also the total number of cells that could be detected on the substrate with these controls was very little, i.e. couple of tens. Ligand patch spacing (●) and projected cell area (□) 23 h after cell plating as a function of substrate position, when the spacing range of c(-RGDfK-) patches covers (d) 45−65 nm, gradient strength Δ80 nm/mm, and (e) 80−110 nm, gradient strength Δ15 nm/mm.

larger molecular weight of PS resulted in a wider particle spacing range by gradual variation of the substrate retraction velocity. Particle spacing gradients with different strengths of Δ19 ± 1, Δ30 ± 3, and Δ50 ± 7 nm/mm were obtained by varying the acceleration of the retraction speed (Figure 1d). The insets show SEM micrographs of highly regular gold nanopatterns at a substrate position below 3 mm and above 5 mm. Figure 1e depicts particle spacing gradients of different directions on the same substrate.

The nanoparticle spacing gradients were applied to measure the sensitivity of adherent tissue cells to variations in spatial presentation of adhesive ligand "nanopatches", whereby each patch may bind up to one integrin molecule. Therefore, the substrate area which was not covered by gold nanoparticles was passivated by polyethylene glycol (PEG) to avoid nonspecific protein adsorption.[5,25] The nanoparticles were functionalized with the c(RGDfK)-thiol cell adhesive molecules, which specifically bind to integrins.[5,9] Accordingly, each functionalized nanoparticle served as a c(-RGDfK-) adhesion patch. The patch size was approximately 8 nm, that is, 6 nm diameter of the gold particle, plus a 2 nm layer formed by the c(-RGDfK-) layer. Therefore, each c(-RGDfK-) patch presented a single binding site for up to one integrin due to steric hindrance when cells were plated on the nanostructured support (Figure 2a).[20] In former publications, we demonstrated that nonfunctionalized nanogold particles[5] or particles that were functionalized with a peptide presenting a random chosen sequence, that is, RGE,[9] did not induce any adhesion associated cell response. Even in the case of blocking the cell adhesion receptor integrin $\alpha v\beta 3$ with antibodies but functionalizing the nanogold particle array with c(-RGDfK-), no adhesion of cells was found which proved the specificity of the surface functionalization concept once more.[8] The height of the nanoparticles was adjusted such that it matches the height of the PEG layer between the nanogold particles, that is, approximately 6 nm. Thus, potential topographical effects did not account for cell adhesion associated response.[5,25] Figure 2b−d shows high-resolution SEM micrographs which display cells' haptic sensitivity at the nanometer scale. Small cell protrusions of 10−20 nm are associated with single c(-RGDfK-) adhesion patches of 8 nm diameter.

The c(-RGDfK-) functionalized nanoparticle spacing gradient was applied to screen for changes in cellular morphology as a result of c(-RGDfK-) patch interspacing. The spacing between c(-RGDfK-) patches was continuously increased from ∼50 nm to ∼80 nm, between positions 3 mm and 5 mm of the substrate (Figure 2e) yielding a gradient strength of ∼Δ15 nm/mm. High-magnification phase-contrast micrographs (Figure 2e) indicate that the cell morphology changed from radial, well-spread adherent cells at a ligand patch spacing of ∼50 nm, to strongly elongated cells at a spacing of ∼80 nm.

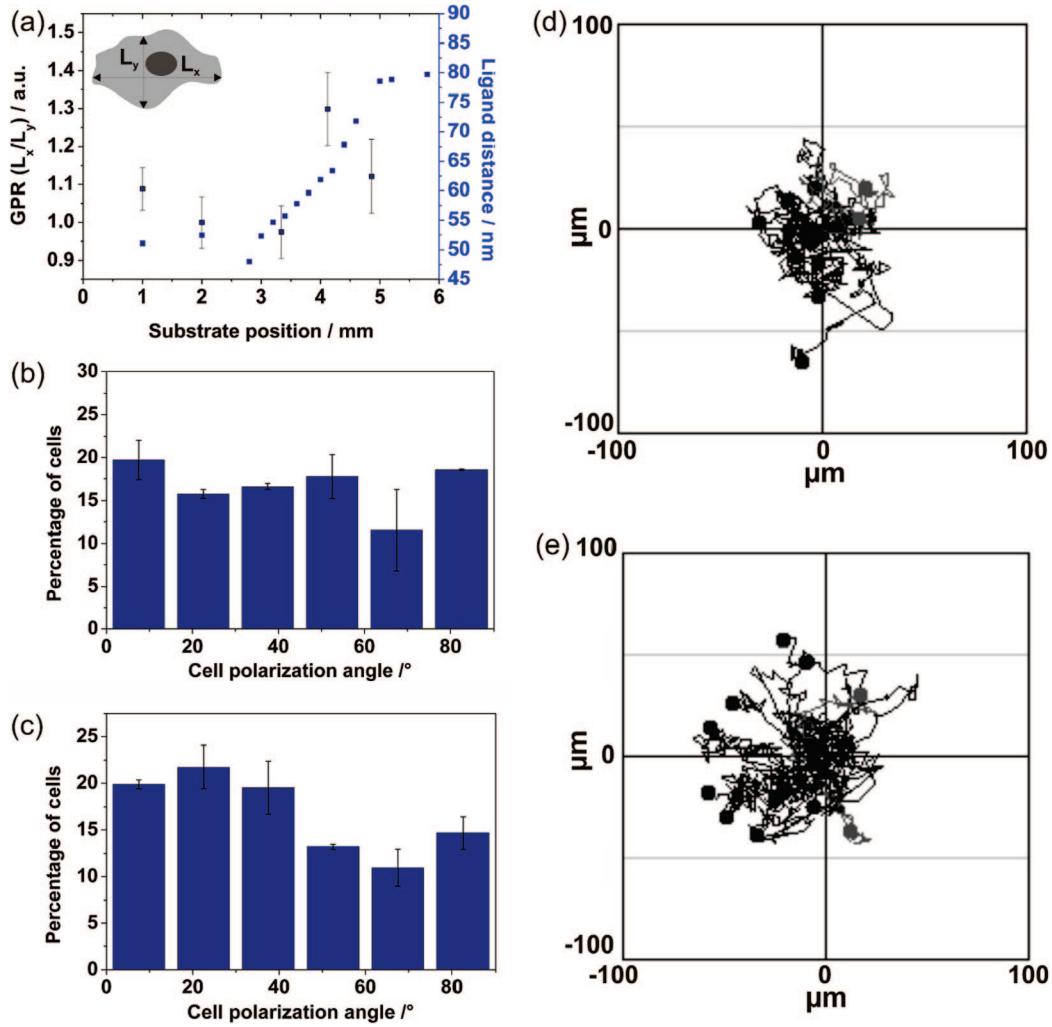

Figure 4. Morphological analysis of MC3T3 osteoblasts in contact with ligand patch spacing gradients. (a) GPR-value (black ■) and ligand patch spacing (blue ■) as a function of substrate position for cells adhering to a gradient with a strength of Δ15 nm/mm. Cell polarization angle distribution of MC3T3 osteoblasts adhering to areas which consist of (b) a constant ligand patch spacing of ∼50 nm and (c) a gradient as documented in (a) (0° = cells oriented along the gradient; 90° = cells oriented perpendicular to the gradient). REF fibroblast migration paths on areas which present (d) a constant ligand patch spacing of ∼60 nm; and (e) a ligand patch gradient with a strength of Δ25 nm/mm covering 60 to 110 nm spacing. For migration studies cells were cultured for 13 h on the respective substrates and then imaged every 10 min for 12 h.

The dynamic response of cells to a c(-RGDfK-) interparticle spacing gradient was documented by analyzing the projected cell area after 2.5, 8, and 23 h in several substrate positions (Figure 3a−c). After 2.5 h, most cells were round and did not show a significant morphological variation along the gradient. The locally measured projected cell area was scattered around the mean projected cell area of 1500 μm^2. Eight hours after plating, an increase in cell area along the gradient from ∼1500 to ∼2250 μm^2 for smaller patch spacing could be noted. After 23 h, position-dependent variations in cell spreading were clearly detected as a function of variations in spacing. On the dense part of the substrate, cells maintained a size of ∼2250 μm^2, while those attaching to c(-RGDfK-) interpatch distances of 70 nm or more decreased their projected cell area even further, to a final size of ∼1000 μm^2. Undoubtedly, cells response was due to gradual variations in c(-RGDfK-) interpatch distances since nonfunctionalized nanogold particles or particles that were functionalized with the RGE peptide did not at all indicate any comparable response (Figure 3c). In general, it was rather difficult to find cells which remain at the nanopattern substrates if the pattern was not functionalized with c(-RGDfK-). The couple of ten cells which were still discovered along the substrate were mainly spherical in shape and not spread. Evaluation of their mean projected cell area gave values below 250 μm^2 per cell (Figure 3c). It is noteworthy that projected cell areas of spherical cell do not recall their adhesion area. Even more, we claim that these couples of cells were attached to the substrates only because of defects in the substrate. In contrast, c(-RGDfK-) functionalization of the pattern obtained adhesion and spreading of couples of hundred cells with obviously much larger projected cell areas than in the other mentioned nanogold functionalization experiments. Only a slight linear decrease in the projected cell area was observed for spacing values which did not include a 70 nm distance, that is, gradients ranging from 45 to 65 nm with a gradient strength of Δ40

nm/mm (Figure 3d) or 80−110 nm with a gradient strength of Δ15 nm/mm (Figure 3e).

Another morphometric parameter of adherent cells is the degree of cell polarization, obtained by calculating the gradient polarization ratio (GPR), defined as the axial ratio of the most extended width of the cell body along the gradient (L_x) and the most extended width of the cell body perpendicular to the gradient (L_y; Figure 4a). In general, a GPR value of ∼1 represents cells with no polarization, while a GPR > 1 indicates cells that are polarized. The GPR values are plotted here as a function of the substrate position. Within the error margins, the evaluated GPR values of MC3T3 osteoblasts at a homogeneous distributed ligand patch spacing of ∼50 nm are constant and show a typical value of ∼1. The strongest polarization of cell bodies occurred in the middle of the gradient with a value of ∼1.3, where the patch spacing range is between 60 and 70 nm. The orientation angle distribution of elongated cell bodies is given in Figure 4b,c. In the case of a constant ligand patch spacing of 50 nm, cells did not choose a preferred orientation, even after 21 h. However, along the c(-RGDfK-) patch spacing gradient, cells polarized with a preferred angle, relative to the direction of the gradient, between 0 and 30°. Cell polarization was often accompanied by directional cell migration along the gradient. REF fibroblast migration tracks are plotted in Figure 4d,e; approximately 15 different cells in each plot may be seen. While cells on a homogeneous ligand patch spacing of ∼60 nm navigated in all directions with the same probability, cells navigating on a ligand patch spacing gradient of ∼Δ25 nm/mm (covering 60 to 110 nm spacing) obviously sense the gradient and migrate in the direction of smaller spacing (toward the left in Figure 4e).

The weakest gradient to which cells responded had a strength of Δ15 nm/mm, if the gradient included the 70 nm spacing. Under these conditions, cells displayed an average length of $\langle L_x \rangle \sim 61 \pm 3\ \mu$m in the direction of the gradient. A cell thus elongated along the gradient is exposed and can respond to a difference in ligand patch spacing of ∼0.9 ± 0.5 nm between the cell's front and rear. This sensitivity to such a small length scale is remarkable, being much smaller than the expected "noise" and is, most likely, achieved in a time-integrative manner. This sensitivity may only be realized with molecular operations such as optimal receptor clustering. One may speculate that this exquisite cellular sensitivity arises from conditions prevailing in vivo, such as the 67 nm periodicity given in collagen, which forms 80% of the environment of tissue cells.[26] Therefore, our findings also address the precise conditions with which cellular environments must be constructed in order to sustain structure and function of living tissues.

In summary, the development of a novel nanoscale ligand spacing gradient enabled us to study the high sensitivity of tissue cells to changes in spatial presentation of adhesion ligand patches. Particle spacing gradients of varying strengths and a spacing range covering 50 to 250 nm were demonstrated with gold nanoparticles of approximately 6 nm in diameter. Specific biofunctionalization of the particle spacing gradient enabled us to determine the minimal gradient strength required in order to make cells polarize, that is, Δ15 nm/mm gradient strength. Since each gold nanoparticle functionalized by c(-RGDfK-) peptides offers a single binding site for the adhesion receptor integrin, a gradual increase in particle spacing tests the importance of receptor clustering-based responses in the ability of cells to sense spatial variations of <1 nm, presented by the extracellular matrix.

Acknowledgment. We wish to thank Thorsten Brach for technical assistance and Dr. Philippe Girard and Prof. Jennifer Curtis for writing the SEM image analysis program. The Landesstiftung Baden-Württemberg and the Max-Planck-Society are acknowledged for their financial support. This publication and the project described herein were also partly supported by the National Institutes of Health through the NIH Roadmap for Medical Research (PN2 EY 016586). Its contents are solely the responsibility of the authors, and do not necessarily represent the official views of the NIH or the National Eye Institute, which administers this program. B.G. holds the Erwin Neter Professorial Chair in Cell and Tumor Biology. M. López-García thanks Alexander von Humboldt Foundation for a postdoctoral fellowship. We would also like to thank the International Graduate School of Science and Engineering (IGSSE).

References

(1) Geiger, B.; Bershadsky, A.; Pankov, R.; Yamada, K. M. *Nat. Rev. Molecular Cell Biology* **2001**, *2* (11), 793–805.
(2) Meyer, A.; Auernheimer, J.; Modlinger, A.; Kessler, H. *Curr. Pharmaceut. Des.* **2006**, *12* (22), 2723–2747.
(3) Chen, C. S.; Mrksich, M.; Huang, S.; Whitesides, G. M.; Ingber, D. E. *Science* **1997**, *276* (5317), 1425–8.
(4) Discher, D. E.; Janmey, P.; Wang, Y. L. *Science* **2005**, *310* (5751), 1139–43.
(5) Arnold, M.; Cavalcanti-Adam, E. A.; Glass, R.; Blummel, J.; Eck, W.; Kantlehner, M.; Kessler, H.; Spatz, J. P. *Chemphyschem* **2004**, *5* (3), 383–8.
(6) Haubner, R.; Gratias, R.; Diefenbach, B.; Goodman, S. L.; Jonczyk, A.; Kessler, H. *J. Am. Chem. Soc.* **1996**, *118* (32), 7461–7472.
(7) Cavalcanti-Adam, E. A.; Micoulet, A.; Blummel, J.; Auernheimer, J.; Kessler, H.; Spatz, J. P. *Eur. J. Cell Biol.* **2006**, *85* (3−4), 219–24.
(8) Cavalcanti-Adam, E. A.; Volberg, T.; Micoulet, A.; Kessler, H.; Geiger, B.; Spatz, J. P. *Biophys. J.* **2007**, *92* (8), 2964–74.
(9) Hersel, U.; Dahmen, C.; Kessler, H. *Biomaterials* **2003**, *24* (24), 4385–415.
(10) Plummer, S. T.; Wang, Q.; Bohn, P. W.; Stockton, R.; Schwartz, M. A. *Langmuir* **2003**, *19* (18), 7528–7536.
(11) Kang, C. E.; Gemeinhart, E. J.; Gemeinhart, R. A. *J. Biomed. Mater. Res. A* **2004**, *71* (3), 403–11.
(12) Dertinger, S. K.; Jiang, X.; Li, Z.; Murthy, V. N.; Whitesides, G. M. *Proc. Natl. Acad. Sci. U.S.A.* **2002**, *99* (20), 12542–7.
(13) Maheshwari, G.; Brown, G.; Lauffenburger, D. A.; Wells, A.; Griffith, L. G. *J. Cell Sci.* **2000**, *113* (Pt 10), 1677–86.
(14) Herbert, C. B.; McLernon, T. L.; Hypolite, C. L.; Adams, D. N.; Pikus, L.; Huang, C. C.; Fields, G. B.; Letourneau, P. C.; Distefano, M. D.; Hu, W. S. *Chem. Biol.* **1997**, *4* (10), 731–7.
(15) Jiang, X.; Xu, Q.; Dertinger, S. K. W.; Stroock, A. D.; Fu, T.-m.; Whitesides, G. M. *Anal. Chem.* **2005**, *77* (8), 2338–2347.
(16) Kraus, T.; Stutz, R.; Balmer, T. E.; Schmid, H.; Malaquin, L.; Spencer, N. D.; Wolf, H. *Langmuir* **2005**, *21* (17), 7796–7804.
(17) Lee, K.-B.; Park, S.-J.; Mirkin, C. A.; Smith, J. C.; Mrksich, M. *Science* **2002**, *295* (5560), 1702–1705.
(18) Bhat, R. R.; Fischer, D. A.; Genzer, J. *Langmuir* **2002**, *18* (15), 5640–5643.
(19) Kramer, S.; Xie, H.; Gaff, J.; Williamson, J. R.; Tkachenko, A. G.; Nouri, N.; Feldheim, D. A.; Feldheim, D. L. *J. Am. Chem. Soc.* **2004**, *126* (17), 5388–95.

(20) Wolfram, T.; Belz, F.; Schön, T.; Spatz, J. P. *Biointerphases* **2006**, *2* (1), 44–48.
(21) Spatz, J. P.; Moessmer, S.; Hartmann, C.; Moeller, M.; Herzog, T.; Krieger, M.; Boyen, H.-G.; Ziemann, P.; Kabius, B. *Langmuir* **2000**, *16* (2), 407–415.
(22) Glass, R.; Moeller, M.; Spatz, J. P. *Nanotechnology* **2003**, *14* (10), 1153–1160.
(23) Glass, R.; Arnold, M.; Bluemmel, J.; Kueller, A.; Moeller, M.; Spatz, J. P. *Adv.Funct. Mater.* **2003**, *13* (7), 569–575.
(24) Glass, R.; Arnold, M.; Cavalcanti-Adam, E. A.; Blummel, J.; Haferkemper, C.; Dodd, C.; Spatz, J. P. *New J. Phys.* 2004, *6*.
(25) Blümmel, J.; Perschmann, N.; Aydin, D.; Drinjakovic, J.; Surrey, T.; López-García, M.; Kessler, H.; Spatz, J. P. *Biomaterials* **2007**, *94* (4), 1470–1482.
(26) Jiang, F.; Horber, H.; Howard, J.; Müller, D. *J. Struct. Biol.* **2004**, *148* (3), 268–278.

NL801483W